Aerosol hygroscopicity and its link to chemical composition in coastal atmosphere of Mace Head: marine and continental air masses

Wei Xu[1,2], Jurgita Ovadnevaite[1], Kirsten N. Fossum[1], Chunshui Lin[2], Ru-Jin Huang[2,3], Colin O'Dowd[1], Darius Ceburnis[1]

[1]School of Physics, Ryan Institute's Centre for Climate & Air Pollution Studies, and Marine Renewable Energy Ireland, National University of Ireland Galway, University Road, H91CF50 Galway, Ireland

[2]State Key Laboratory of Loess and Quaternary Geology, Center for Excellence in Quaternary Science and Global Change, and Key Laboratory of Aerosol Chemistry and Physics, Institute of Earth Environment, Chinese Academy of Sciences, 710061 Xi'an, China

[3]Open Studio for Oceanic-Continental Climate and Environment Changes, Pilot National Laboratory for Marine Science and Technology (Qingdao), 266061Qingdao, China

Correspondence to: Ru-Jin Huang (rujin.huang@ieecas.cn) and Colin O'Dowd (colin.odowd@nuigalway.ie)

Abstract. Chemical composition and hygroscopicity closure of marine aerosol in high time resolution has not been yet achieved because of the difficulty in measuring refractory sea-salt concentration in near-real time. In this study, attempts were made to achieve a closure for marine aerosol based on a humidified tandem differential mobility analyser (HTDMA) and a high-resolution time-of-flight aerosol mass spectrometer (AMS) for wintertime aerosol at Mace Head, Ireland. The aerosol hygroscopicity was examined as a growth factor (GF) at 90 % relative humidity (RH). The corresponding GFs of 35, 50, 75, 110 and 165 nm particles were 1.54 ± 0.26, 1.60 ± 0.29, 1.66 ± 0.31, 1.72 ± 0.29 and 1.78 ± 0.30 (mean ± standard deviation), respectively. Two contrasting air masses (continental and marine) were selected to study the temporal variation in hygroscopicity and the results demonstrated a clear diurnal pattern in continental air masses, while no diurnal pattern was found in marine air masses. In addition, the winter time aerosol was observed to be largely externally mixed in both contrasting air masses. Concurrent high time resolution PM_1 (particulate matter < 1 µm) chemical composition by combined AMS and MAAP measurements comprising of organic matter, non-sea-salt sulphate, nitrate, ammonium, sea-salt and black carbon (BC) were used in predicting aerosol hygroscopicity using the Zdanovskii–Stokes–Robinson (ZSR) mixing rule. A generally good agreement ($r^2 = 0.824$, slope = 1.02) was found between HTDMA measured growth factor (GF_HDTMA) of 165 nm particles and AMS+MAAP bulk chemical composition derived growth factor (GF_AMS). Over 95% of the estimated GF exhibited less than 10% deviation for the whole dataset and the deviation was mostly attributed to the neglected mixing state as a result of bulk PM1 composition.

1. Introduction

Marine aerosol is probably the most important component of natural aerosol in terms of climate effect (O'Dowd and de Leeuw, 2007), because over 70% of the Earth's surface is covered by world oceans. There are two ways that marine aerosol can exert its impact on global climate, one by scattering the incoming solar radiation, and the other by acting as cloud condensation nuclei (CCN). Hygroscopicity - the ability of water vapor uptake by aerosol, plays a significant role for both. Hygroscopicity affects the mass of aerosols by increased aerosol liquid water content and enhances particle light scattering, therefore, cooling the atmosphere directly. Furthermore, hygroscopicity has a large impact on CCN activation and cloud droplet formation, modifying cloud radiative forcing and the hydrological cycle (Twomey, 1974; 1977).

Aerosol hygroscopicity is determined by its chemical composition. Closure studies which attempted to predict hygroscopicity based on chemical composition measurements have improved understanding of the relationship between aerosol hygroscopicity and chemical composition in various environments. Thanks to the wide use of aerosol mass spectrometry (AMS), chemical composition of aerosols is now available to attempt closure with hygroscopicity data in a high time resolution. For example, closure study conducted in Paris revealed an over-estimation of predicted hygroscopicity when nitrate mass concentration exceeded 10 $\mu g \ m^{-3}$ (Kamilli et al., 2014). A closure study in Beijing suggested that the hygroscopicity of organics was related to their oxidized state (Wu et al., 2016), while another study in Hongkong did not find any improvement in closure (Yeung et al., 2014). Despite the advantage of collocated aerosol chemical composition and hygroscopicity measurements helping to reconcile sub-saturated particle hygroscopicity with its chemical composition thereby identifying knowledge gaps, it is widely accepted that sea-salt (the main component of marine aerosol) measurements by AMS are challenging because of its semi-refractory nature resulting in incomplete chemical composition and unrealistic hygroscopicity. The hygroscopicity of marine aerosol has been intensively studied, including studies in the Arctic (Zhou et al., 2001), Atlantic (Swietlicki et al., 2000) and Pacific (Berg et al., 1998) oceans, but chemical composition and hygroscopicity closure studies are still very limited. A hygroscopicity and chemical composition study conducted in the Northeastern Pacific (Kaku et al., 2006) found over 30% overestimation of growth factor (GF) by using the Zdanovskii–Stokes–Robinson (ZSR) mixing rule. The study speculated that the overestimation was caused by the non-ideal behavior of organics. Investigation into the hygroscopicity of aerosol in Antarctica by using an impactor for size-segregated composition of marine aerosol particles, found the hygroscopicity mainly driven by inorganic salts (Asmi et al., 2010). However, due to the limitation of sampling technique (filters and impactors) and a short sampling period, they were unable to capture the temporal evolution of chemical composition, hindering the detailed analysis of real time linkage to hygroscopicity.

This study aimed at characterizing marine and continental aerosol during winter period of low marine biological productivity at the coastal Mace Head Atmospheric Research Station situated at the boundary of the North East Atlantic and rural West of Ireland. The aerosol hygroscopicity was measured in-situ in sub-saturated conditions (RH 90%) using a humidified tandem differential mobility analyzer (HTDMA). Aerosol hygroscopicity parameter was also estimated using chemical composition data using near real-time chemical composition measurements including sea-salt by a high-resolution time-of-flight aerosol

mass spectrometer (HR-ToF-AMS) and Multiple Angle Absorption Photometer (MAAP). Two contrasting cases were analyzed in detail to represent continental and marine air masses in which the hygroscopic aerosol properties were expected to differ greatly. To the best of our knowledge, this is the first closure study on aerosol hygroscopicity and chemical composition including sea salt for marine aerosols in high time resolution.

70

2. Method

2.1 Site Description

The Mace Head Atmospheric Research Station is located on the North Atlantic coast of Ireland, co. Galway at 53°19′36″N, 9°54′14″W (O'Connor et al., 2008). Air is sampled from the main community sampling duct which draws air from 10 m above

75   ground level and is positioned 80-120 m from the ocean depending on the tide. Meteorological data is recorded at the station, including rainfall, solar radiation, wind speed, wind direction, temperature, RH, and pressure (available at www.macehead.org). The measurements were conducted from 1st Jan to 23rd March 2009 and comprised of 1300 hours of valid HTDMA and AMS data. Air masses were tracked using HYSPLIT (Rolph et al., 2017) 72 h backward trajectories with an endpoint of 500 m above mean sea level at Mace Head with Global Data Assimilation System (https://www.ncdc.noaa.gov/data-access/model-

80   data/model-datasets/global-data-assimilation-system-gdas).

2.2 Instrumentation

2.2.1 HTDMA

The hygroscopic growth factor of aerosol particles was measured with an HTDMA (Liu et al., 1978; Rader and McMurry, 1986; Swietlicki et al., 2008 ; Tang et al., 2019). The HTDMA at Mace Head which was described in great detail in previous

85   studies (Bialek et al., 2012; 2014) consisted of a dry Hauke-type differential mobility analyzer (DMA, RH<10%, dried by a Nafion^{TM} dryer), Gore-Tex^{TM} humidifier, second Hauke-type DMA and a condensation particle counter (CPC, TSI model 3772). To stabilize the RH the second DMA was placed in a temperature-controlled box. Four Rotronic RH/temperature sensors and an Edgetech Dewmaster dewpoint chilled mirror sensor were used to monitor the RH fluctuation within the system and the humidifier was controlled by an analogue to digital and digital to analogue feedback system. The first DMA was used

90   to select monodisperse particles with a certain electrical mobility. The monodisperse particles were then humidified and hygroscopicity growth probability distribution function is then produced by the second DMA and the CPC. Since the dry diameter of aerosol is well established, the hygroscopic growth factor can be calculated by measuring the aerosol size distribution at selected RH. To retrieve growth factor from raw data, and to correct the broadening of DMA distribution, a piece linear inversion algorithm was used (Gysel et al., 2009). In this study, the first DMA was constantly at an RH 10%, while

95   the second DMA was set at RH=90%. The dry particle diameters selected by the first (dry) DMA were 35, 50, 75, 110 and 165 nm, with a scan duration of 180 seconds such that the full cycle through all diameters took 15 minutes. The sample and sheath flow rates were 1 L min^{-1} and 9 L min^{-1}, respectively. The operation and quality assurance procedure followed standard

configuration and deployment recommended by the European Supersites for Atmospheric Aerosol Research (EUSAAR) network project (Duplissy et al., 2009).

2.2.2 Chemical composition (HR-ToF-AMS and MAAP)

The chemical composition was measured using HR-ToF-AMS (Aerodyne Research Inc. Billerica, MA) (DeCarlo et al., 2006) which has a vacuum aerodynamic cut-off diameter of 1 µm. Regular calibrations with ammonium nitrate were performed and the composition-dependent collection efficiency was applied. The AMS provided the mass concentration of organic matter, ammonium, non-sea-salt sulfate, nitrate, methanesulfonic acid (MSA). The AMS typically runs at evaporation temperature of 600 °C, which is optimized for the detection of non-refractory aerosols species such as organic matter, nitrate, sulfate and ammonium. Sea salt was expected to be refractory at the above temperature and thereby compromising detection of non-refractory species (Allan et al., 2004). However, Ovadnevaite et al. (2012) has convincingly demonstrated that sea salt can be successfully quantified at the standard evaporation temperature as long as relative humidity is maintained within reasonable limits ($< 80\%$) and the AMS vaporizer is not overloaded by sea salt. In this study, the sea-salt which was retrieved by using a $^{23}Na^{35}Cl^+$ ion signal at m/z 58 and a scaling factor of 51 (Ovadnevaite et al., 2012). The quantification of MSA was realized and calibrated by ion signal $CH_3SO_2^+$ and $CH_3SO_3H^+$ which are the exclusively related to MSA. The composition dependent collection efficiency (CDCE) was used to correct AMS species concentrations (Middlebrook, Bahreini et al. 2012). CDCE does not take into account sea salt nor organic matter contribution; however, those species would only be corrected proportionally to the total mass (if at all) and would not affect fractional contribution of species which is used in this study. We attempted a comparison between SMPS volume and AMS plus BC combined volume to attest the CDCE correction. The comparison is presented in Figure S1 (the slope was 1.03 ± 0.01). The excellent agreement in volume comparison suggested that CDCE correction was realistic with few outliers pointing at slight size range discrepancy between SMPS and AMS. The relationship between sea salt and wind speed is presented in Figure S2 for the entire year of 2009 and was similar to the one previously published by Ovadnevaite et al. (2012) although not as clear-cut as previously published. It must be noted that despite the wind speed being the dominant factor for sea salt aerosol production, there were few more parameters in the sea spray source function related to the sea state, salinity and temperature, all affecting the quantitative relationship. The excellent agreement can only be expected in very well-defined low pressure systems producing sea salt events where sea salt is well mixed and filled in the entire boundary layer as it only happens during significant storms. While the sea spray source function is at work during every occasion of wind speed induced bubble bursting, quantitative representation of particle mass and number is not instantly achieved. Nevertheless, both relationships provided extra confidence on the quantitative detection of sea salt by AMS. Nevertheless, both relationships provided extra confidence on the quantitative detection of sea salt by AMS.The operational details of the HR-ToF-AMS are described by Ovadnevaite et al. (2014). The degree of neutralization of bulk aerosol was calculated as: $DON = \frac{n(NH_4^+)}{2nSO_4^{2-} + nNO_3^-}$. The concentration of optically absorbing black carbon (BC) was measured by a Multi-Angle Absorption Photometer (MAAP, Thermo Fisher Scientific model 5012). The MAAP operated at

130 a flow rate of 10 L min^{-1} at 5 min time resolution. The MAAP measured transmittance and reflectance of BC contained particles at two angles to calculate optical absorbance, as described in Petzold and Schönlinner (2004).

2.3 Hygroscopicity data analysis

The growth factor (GF) of aerosol particles undergoing humidification was obtained by: $GF = \frac{D}{D_0}$, where D and D_0 are the

135 electrical mobility diameters of humidified and dry aerosols, respectively.

One of the HTDMA features is the ability to reveal aerosol mixing state by detecting the presence of more than one particle growth mode. Each growth mode represents different water uptake properties, indicating a different chemical composition of each mode. The growth factor probability distribution function was separated into four growth modes according to their GF range: Near Hydrophobic mode (NH, 1< GF< 1.11), Less Hygroscopic mode (LH, 1.11< GF< 1.33), More Hygroscopic mode

140 (MH, 1.33< GF< 1.85) and Sea Salt mode (SS, 1.85< GF). For particles in a specific GF range, for example LH, the number fraction of this mode (nf_LH) was derived from the retrieved probability density function c(GF, D) as: nf_LH = $\int_{1.11}^{1.33} c(GF, Do) gGF$. It should be noted that this categorization was not always representative. For example, in highly acidic marine aerosol, the MH mode peaked at 1.8< GF< 2.0 resulting from high highly hygroscopic H_2SO_4 with GF up to 1.9 rather than sea salt. Due to the spread of GF-PDF, some sections of PDF representing non-neutralized particles could be categorized

145 into SS mode, which would then result in underestimation of averaged GF for both MH and SS modes, and overestimation of the number fraction of SS mode. The GF$_{mean}$ of each mode was calculated as: $GF_{mean} = \frac{1}{nf^{a,b}} \int GF\, c(GF, D) dGF$

2.4 Hygroscopicity-Chemistry Closure

150 The mass concentrations were converted to volume fractions of individual components (organics, NH_4HSO_4, H_2SO_4, NH_4NO_3, $(NH_4)_2SO_4$, MSA, sea-salt and BC) by using a simplified ion pairing scheme (Gysel et al., 2007). The GFs values of individual components are summarized in Table 1. Although the hygroscopicity of inorganic compounds is well understood and established, it is still challenging to quantify the hygroscopicity of organic matter ranging from 1 to 1.5 or from hydrocarbon to oxalic acids (Kreidenweis and Asa-Awuku, 2014), however, most of the anthropogenic organics have GF <1.2. In this study,

155 we first used a fixed GF value of 1.18 for organics which was the averaged value from several closure studies (Wang et al., 2018; Yeung et al., 2014) and a constant density of 1400 kg m^{-3} used by Gysel et al. (2007).

Assuming a constant GF and density value for organics may induce a bias for closure studies because the hygroscopicity of organics differs according to their molecular structure, air mass history, or oxidation level. The GF$_{MSA}$=1.71 was calculated by kappa value which in turn was obtained by AIOMFAC model (Fossum et al., 2018; Zuend et al., 2011) and supported by a

160 recent lab experiment (Tang et al., 2018). The hygroscopicity of inorganic sea-salt was found to be 8-15% lower than that of pure NaCl, therefore, a GF value 2.22 of inorganic sea-salt (at RH 90%) was used (Zieger et al., 2017). The closure between

the measured and predicted values was characterized by a linear regression and the corresponding values of R^2 (the variance, which is a square of the correlation coefficient) and regression slope.

Growth factor estimation was based on the Zdanovskii-Stokes-Robinson (ZSR) mixing rule (Stokes and Robinson, 1966) using measured aerosol chemical composition, which assumes that water uptake of the mixture is equivalent to the sum of the water uptake of individual substances. GF calculated from the bulk chemistry of the HR-ToF-AMS(GF_AMS) can be written as: $GF\_AMS = \sum_i v_i GF_i$, where v_i is the volume fraction of the compound in the dry particle, and GF_i is the growth factor of the individual chemical components. In the above equation, any interaction between the solutes is neglected and the volume of the dry mixture is the sum of the volumes of its dry components.

3. Result and Discussion

3.1 Meteorology and air mass origin

The measurement period spanned from the 1st January 2009 to the 23rd March 2009. Data including meteorological parameters and aerosol chemical composition are shown in Fig 1. The average ambient temperature and RH for the entire period were 6.5 $\pm$ 2.5 $^{\circ}$C and 85.8 $\pm$ 8.8 %, respectively.

The measurement period was examined in terms of contrasting air mass origin and two continental events (C1, C2) and two marine events (M1, M2) were selected. These contrasting events are highlighted in the time series shown in Fig. 1 and were expected to reveal greatly different hygroscopic properties of aerosol particles. The air mass backward trajectories for these four events are shown in Fig. 2. Events C1 and C2 represented air masses which originated over continental Europe 72 hours prior to being transported across the UK and Ireland towards Mace Head. Events M1 and M2 were considered representing clean marine air originating over the North East Atlantic Ocean and transported to the west coast of Ireland. The start and end time of each event is summarized in Table S1. The mass concentrations of chemical composition, including non-sea-salt sulfate, nitrate, ammonium, organic, MSA, sea-salt and black carbon of each event are summarized in Table S2. It is important to emphasize that marine air masses are not always pristinely clean despite of advecting over the oceanic waters. Therefore, only data with BC <15 ng m^{-3} and wind direction within the 190 to 300° sector were included in data analysis of marine events and subsequently summarised in Table S2. The mean BC concentrations during M1 and M2 events were 10.1 and 9.9 ng m^{-3}, respectively, demonstrating the value of conservative approach to qualifying pristine marine air masses and the corresponding data capture is presented in Figure S3 for M1 event. The strict and conservative BC criterion has been used to filter the cleanest maritime air masses. An analysis of the representativeness of clean maritime air masses has been extensively discussed by O'Dowd et al. (2013) where no correlation was found between organic matter (OM) and BC for different BC concentration ranges of 0 -15 ng m^{-3}, and 15 -50 ng m^{-3} ($R^2 = 0.006$ and $R^2 = 0.046$, respectively). Figure S8 showing the non-refractory organics and non-sea-salt sulfate concentration by AMS versus BC concentration in this study again demonstrating no relationship in

clean marine air masses using conservative BC criterion. However, there was a relationship between the species in continental air masses as one would expect where pollutants are typically internally mixed and advected by long-range transport to the site.

3.2 Aerosol hygroscopicity

3.2.1 Overview of hygroscopicity measurements

During the full winter measurement period, aerosols displayed temporal variation in GF-PDF across all sizes, and overall the larger particles clearly exhibited larger GF values (Fig. 3). The mean GF of 35, 50, 75, 110 and 165 nm dry mobility diameter particles were 1.54 ± 0.26, 1.60 ± 0.29, 1.66 ± 0.31, 1.72 ± 0.29, 1.78 ± 0.30, respectively.

The GF-PDFs were observed to be highly size dependent throughout the sampling period (Fig. 3) and, in addition, different modal pattern (single mode, bimodal and/or trimodal) were found for all measured particle sizes but of different frequency of occurrence. The occurrence of single mode profiles increased with decreasing D_0 size, such as the frequency of occurrence was 10.4 % for 35 nm particle diameter, 8.8 % for 50 nm, 7.6 % for 75 nm, 4.7 % for 110 nm and 3.0 % for 165 nm dry particle diameter. A few trimodal patterns were observed, particularly in marine air masses, and the occurrence of trimodal profiles similarly increased with decreasing size, such as the frequency of occurrence was 9.8% for 35 nm, 7.9 % for 50 nm, 6.5% for 75 nm, 3.8% for 110 nm and 1.9% for 165 nm dry particle diameter. Overall, bimodal GF-PDF profiles dominated the whole winter period regardless of size (Fig. 3), suggesting that the sampled aerosol was largely externally mixed at Mace Head during the entire winter season. To determine the influence of air mass, we examined the hygroscopicity and chemical composition of marine and continental aerosol in the following sections.

3.2.2 Continental air masses

No precipitation was observed during continental air mass events, and measured temperatures were typical of Mace Head winter seasons, ranging from 1 to 6 °C, while RH ranged from 70 to 100%. Wind speed peaked at a maximum of 17 m s^{-1} and a minimum of below 5 m s^{-1}.

Figure 3 provides an overview of the GF-PDFs and average GFs of pre-selected aerosol particles. Throughout the C1 and C2 events, particles with a dry size $D_0 > 75$ nm exhibited bimodal or trimodal GF-PDFs with a mode of more-hygroscopic and a mode of less hygroscopic or a mode of near hydrophobic nature. Particles with sizes $D_0 < 50$ nm were rather different and dominated by LH mode and NH modes. Completely non-hygroscopic particles (GF ~ 1) were not observed, but some of the GF-PDF data spread reached NH mode, indicating some extent of internal mixing, however, dominant multimodal pattern clearly demonstrated mostly external mixing. External mixing has also been observed in other studies in winter, especially in locations with large anthropogenic influence (Swietlicki et al., 2008).

Figure 4 depicts the number fraction of each growth mode type by measured particle size over the winter measurement period. The MH mode was dominated by 165 nm particles, while the LH mode and NH mode became more prominent as the size decreased. A similar size dependence mode distribution was also observed in Beijing (Wu et al., 2016) and the southern

Sweden (Fors et al., 2011). The number fraction of NH (nf_NH) were similar for all sizes, nf_LH decreased with increasing particle size nf_MH mode increased with increasing size. It is generally argued that larger particles have typically undergone atmospheric aging and cloud processing (such as coagulation, droplet coalescence, condensation of semi-volatile gases, chemical reactions and photo-oxidization) for a longer period of time thus acquiring additional mass, growing in size and exhibiting more hygroscopic features. The SS mode was very small in continental air masses as expected (frequency of occurrence of 1 % during C1 and 5 % during C2), but externally mixed sea-salt was clearly discerned nevertheless. As shown in Fig. S4, the average GF of 110 nm and 165 nm particles showed a clear diurnal pattern, which peaked at about 11:00 every day and reached a minimum at 20:00. This trend was similar to the GF observation in Po Valley (Bialek et al., 2014) or Oklahoma site (Mahish and Collins, 2017) and is often attributed to a shallower and more stagnant boundary layer during the night with temperature inversions arising from radiative cooling of the surface. When the sun rises in the morning, the boundary layer increased in height and the older particles are mixed down. In general, the old particles are more hygroscopic resulting from the cloud processing and photo-aging (Rissler et al., 2006).

The AMS and MAAP measurements are shown in Fig. 1(top), and the mean ± standard deviation of total mass concentration, BC, organic matter, nitrate, ammonium, and non-sea-salt sulfate are shown in Table S2. The mass concentrations of BC, during C1 and C2 were 500 and 518 ng m^{-3}, and nitrate mass loadings were 0.92 and 4.06 µg m^{-3}), suggesting a heavy anthropogenic impact during continental events. The mass concentrations of sea-salt (0.17 and 0.13 µg m^{-3}), suggesting little impact of marine sources during C1 and C2 during winter.

3.2.3 Marine air masses

Aerosol hygroscopicity in the marine air masses was dramatically different from the continental air masses. The meteorological conditions and chemical composition of each event are shown in Fig. 1. During marine air mass events M1 and M2, the wind speed varied from 4 to 20 m s^{-1}, wind direction varied from 180- 320° and corresponded to clean maritime conditions at Mace Head (O'Dowd et al. 2014). The RH and temperature ranged from 70-100 % and 0-10 °C, respectively. The marine GF-PDF of M1 and M2 were mostly bimodal, indicating that the aerosol was mostly externally mixed, but generally much more hygroscopic than during continental events. The mean GF of M1 and M2 are shown in Table S3, which ranged from 1.8 to 2.1, suggesting the highly hygroscopic nature of marine aerosol. The diurnal pattern of M1&M2 is shown in Figure S1 and contrary to C1& C2 air masses the M1&M2 did not revealed a clear diurnal pattern, which was likely due to well mixed marine boundary layer and stable temperature over the ocean. Long term data is required to form a solid conclusion which will be the scope of further research.

The MH mode was ubiquitous in wintertime sampled marine aerosol (observed in all scans) along with the SS mode. However, for Aitken mode particles, LH or NH modes were also observed. Quite interestingly, a significant number fraction of sea-salt were detected down to particle diameters of 35 nm in accordance to nanoparticle modes in sea spray source function developed by Ovadnevaite et al. (2014). In this study the greatest number fraction of the SS mode was observed around a particle diameter of 75 nm again in line with the aforementioned sea spray source function. Although the SS mode

observed at 35 nm could have been attributed to sulfuric acid, it was unlikely to be the case in this study for the following reasons: (1) the ammonium tends to react with smaller sulfate particles because of their larger surface to volume ratio producing less hygroscopic ammonium (bi)sufate; (2) highly hygroscopic (GF >1.85) non-sea-salt (or low sea-salt) aerosol has never been observed and (3) the number of SS mode particles (number fraction of SS mode times the number of Aitken mode particles measured by scanning mobility particle sizer) was highly dependent on wind speed. The NH and LH were more pronounced in the smaller sizes. After applying a pristine marine criterion (BC < 15 ng m^{-3} and wind direction within 190 to 300° sector), the NH and LH modes were dramatically reduced across the Aitken mode particles and effectively absent in the accumulation mode particles (Fig. S3), but the NH and LH modes of 35 nm still remained. Given the conservative BC threshold and the absence of low hygroscopicity modes in larger particles local anthropogenic contamination can be excluded. The conclusive origin of less hygroscopic particles observed in the North Atlantic will be the subject of a further long-term study. The GF of MH mode (GF_MH) for Continental and Marine events were summarised in Table S4. The averaged GF_MH also increased with D_0 size (e.g. the GF_MH increased from 1.57 for 35 nm to 1.70 for 165 nm particles for Marine event). The highest GF_MH in 165 nm GF-PDF was around 1.78, which is similar to the GF of ammonium bisulfate (GF = 1.79), indicating that aerosol in the MH mode was largely non-neutralized sulfate originating from marine DMS oxidation and by lack of ammonia resulting in largely acidic particles. Moreover, the marine GF_MH was higher than that of the continental event, which could be attributed to the difference in degree of neutralization. The degree of neutralization for C1, C2, M1, M2 were 0.88, 0.93, 0.24, 0.03, respectively, clearly suggesting a higher contribution of sulfuric acid and ammonium bisulfate in marine air masses. In contrast to previous studies at coastal sites of Hong Kong during winter seasons reporting very low frequency of occurrence of the SS mode (Yeung et al., 2014), our observations indicated a large presence of SS mode during wintertime as a result of long air mass advection over the stormy North Atlantic.

The comparison of GF between continental and marine events is shown in Fig. 5 where GFs increase with aerosol size in both continental and marine events, but the size dependence was rather different. The difference between GFs of 35 and 50 nm was smaller in continental events than that of marine events. On the contrary, the difference among 75, 110 and 165 nm was smaller in marine case events. The size dependence of GF could have resulted from Kelvin effect and (or) chemical composition. To remove the effect of Kelvin effect, the hygroscopicity parameter was calculated. Similar to GFs, the kappa values shown size dependence for both continental and marine events (Fig. S5). The difference size dependence behaviour was the result of different air mass history and corresponding aerosol production mechanisms affecting aerosol chemical composition. Marine aerosols are mainly produced by wind stress induced bubble bursting or gas transfer resulting in secondary particles while continental anthropogenic aerosol underwent significant ageing process being produced by distant man-made sources.

3.3 Chemical composition closure study

The size resolved GFs measured by the HTDMA (denoted as GF_HTDMA) were plotted against GFs estimated by the ZSR mixing rule using AMS chemical composition data (denoted as GF_AMS). The linear regression was used to fit the GF_AMS

and GF_HTDMA, the slope of a nonzero-intercept linear regression fit reflecting how well the estimation agreed with the measurements. As shown in Fig. 6, the regression slopes were 0.91 and 1 for 35 and 165 nm, respectively, and the variance increased from 0.61 to 0.84 with the increase of dry diameter D_0, suggesting the closure agreement getting better for larger sizes. For example, the GF_AMS of 35 nm D_0 aerosols showed an overestimation with over 93% of the data points located outside of the 10% deviation from the 1:1 line. The comparison of 165 nm aerosols to bulk chemistry was very good with over 95% of data points lying within 10% deviation of the 1:1 line. The slope of linear regression is 1.02 suggesting there was no systematic error in GF estimation. The results of the comparison were suggesting that (1) the chemical composition which was used in deriving GF was bulk PM1 data which may differ significantly from Aitken mode particles, but approximating to accumulation mode particles thus affecting poorer comparison of Aitken mode particles and (2) the Kelvin effect, which would become significant at small sizes was neglected in calculation. Contrary to the study of Hong et al. 2018, the correlations between GF_AMS and GF_HTDMA of even small sizes were correlating much better than no-correlation found by (Hong et al., 2018). As described in the method section, the chemical compositions measured by AMS in this study were bulk PM1 chemical composition where contribution of sub-50nm particles was negligible. Consequently, it is expected that the calculated GFs deviates considerably from the measured growth factor for particles smaller than 50 nm. Given the best obtained agreement for the larger sizes, and considering the relevance to the cloud condensation nuclei, we now focus on the closure results of 75, 110 and 165 nm particles to assess event results. As shown in Fig. 6, although a general closure agreement was good, large amount of data points was still scattered around the regression line. Comparison between GF_AMS and GF_HTDMA was plotted for continental and marine events, as shown in Fig. 7.

The regression lines were approaching the 1:1 line with the increasing size. For example, R^2 values were 0.47 and 0.18 for 75 nm particles during continental and marine events. For 165 nm D_0 aerosol, the regression coefficients were 0.72 and 0.54, and the slopes were 1.1 and 0.85 for both continental and marine events.

The regression results were reasonable even for 75nm size, but were certainly getting better with the increasing size for the continental events. However, the improvement was not as significant for marine events (Figure 7). Although a few data points were outside of the 10% deviation range of 75 nm, the R^2 of 75 nm as low as 0.18 due to the lack of dynamic range in GF_AMS, but over 95% of the data were well within 10% and all of the marine events data points were well within 10 % of 1:1 line for 110 and 165 nm. Despite the fact that the above regressions suggested a reasonable closure achieved for continental and marine events, the closure results for each individual event turned out to be different. For 75 nm particles in C1 over 60% of estimated GFs were outside 10% range, while in C2 very few GFs fell outside 10% deviation range. In contrast, for 165 nm particles, C1 GFs were typically overestimated while C2 were underestimated. The above results clearly demonstrated an increasing impact of hydrophobic mode in smaller particles (Figure 4) which was poorly captured by bulk PM1 mass. Marine event GF_HTDMA and GF_AMS were in good agreement, with 95% of data points lying within ±10% of deviation. During individual marine events over 80% of the M1 estimated GFs were underestimated while M2 GFs were mostly overestimated. The regression slope of all the data was 1, indicating that the GF_HTDMA of marine aerosol could be estimated fairly well based on AMS bulk PM1 measurements by using ZSR rule with the sea-salt concentration measured by AMS.

The overall very good agreement was a result of utilising sea-salt mass concentrations derived by AMS (Ovadnevaite et al., 2012). The result verifies AMS as an good technique of near real-time sea-salt measurements. During the selected marine events, the PM1 aerosol volume fraction of sea-salt ranged from 2% to 95%. In our study, the use of high time and mass resolution AMS data and subsequent inclusion of sea-salt mass improved the closure greatly. As far as we are aware, this current chemical composition and hygroscopicity closure study is the first conducted on sea-salt containing aerosol.

3.4 Closure uncertainty and error analysis

Although a general agreement between measured and estimated GF was found in both continental and marine aerosol, the closure results for each event were slightly different and that motivated us to explore the cause of the closure errors focusing on three metrics: (1) O:C ratio, (2) volume fraction of ammonium nitrate (vi(NH_4NO_3)) and (3) aerosol mixing state.

The introduction of a constant GF_{org} was considered to be the cause of a systematic error. The relationship between GF_{org} and organic oxidization level is under intensive debate. In some studies, it was found that GF_{org} increased with increasing O:C ratios in both chamber and ambient studies (Jimenez et al., 2009; Lambe et al., 2011; Massoli et al., 2010; Wong et al., 2011; Wu et al., 2016) and theoretical calculation have demonstrated GF_{org} exhibiting a linear dependence on O:C ratio (Nakao, 2017). However, the correlation between GF_{org} and O:C ratio varied among aerosol sources, and some studies reported no significant relationship (Chang et al., 2010; Suda et al., 2014).

Fig. 8a shows the relationship between O:C ratio and GF deviation by plotting a normalized error |(GF_HTDMA - GF_AMS) / GF_HTDMA|. When O:C ratio was below 0.5, a slight overestimation was observed, but the deviation was less than 10%, however, when the O:C ratio was within the 0.5 to 1.25 range no obvious pattern could be discerned. Freshly emitted hydrocarbon compounds have relatively low O:C ratio and lower hygroscopicity, therefore, a GF_{org} = 1.1 is likely to cause overestimation. When the O:C increases to 0.6, the reported GF_{org} ranges from 1.15 to 1.4 depending on the air mass (Hong et al. 2018).

The introduction of a constant density and constant GF_{org}, may not be valid for every event, and are likely to cause slight overestimation, but cannot explain the larger deviations above 10%, at least for the aerosol observed at Mace Head.

Another reason for the apparent overestimation of GF_AMS was considered to be the evaporation of NH_4NO_3 in the HTDMA instrument, which was implicated in previous closure studies causing closure failure during nitrate enriched periods (Gysel et al., 2007; 2001; Swietlicki et al., 1999). Gysel et al. (2007) reported that 50-60% of the volume of NH_4NO_3 evaporated within the HTDMA for the particle diameter ranging from 50 to 60 nm. Despite this possible cause of the underestimation of GF in the HTDMA, the presence of nitrate is unlikely to be the main cause for discrepancy in our study for several reasons. First, the residence time of aerosols in our HTDMA system is about 10 s, which is significantly shorter than other systems such as the HTDMA in Gysel et al. (2007), which has a residence time of approximately 60 s and resulted in significant NH_4NO_3 evaporation. Second, no obvious correlation was found between GF deviation and a volume fraction (vi) of NH_4NO_3 (R= 0.07, Fig.8 b). Therefore, as far as our study is concerned there is no evidence for ammonium nitrate evaporation responsible for closure discrepancy.

The mixing state of aerosol can influence the hygroscopicity closure in two ways: 1) the accuracy of AMS measurements is determined by the collection efficiency which for internally mixed aerosols is constant for all the particles, while in external mixtures the application of a constant collection efficiency may produce differences between the real and measured chemical species concentration. In addition to that, externally mixed aerosol has size-dependent chemical composition where bulk chemistry will tend to be more representative of larger sized particles (165 nm) that carry the bulk of mass over smaller sized particles (35 nm) which contribute negligibly to mass. While bulk chemical measurements of PM1 mass may induce errors at smaller sizes in external mixtures, internally mixed aerosol would likely show little difference between the bulk chemistry and that of smaller sized particles.

Two metrics were adapted to represent the mixing state: (1) GF spread factor and (2) number fraction of NH and LH modes, nf(NH+LH), both of which were derived from the GF-PDF of 165 nm aerosols. The GF spread factor was defined as the standard deviation of GF-PDF divided by an arithmetic mean GF (Stolzenburg and McMurry, 1988). As the MH mode existed in every event at every particle size, the number fraction of NH and LH (nf(NH+LH)) modes could be used as a metric of the external mixing (Ching et al., 2017; Su et al., 2010). As shown in Fig. 8c and Fig. 8d, the GF spread factor and nf(NH+LH) factor have the largest regression coefficient with GF deviation, the R being 0.51 and 0.57, respectively.

As shown in Fig. 8c, when GF spread factor is less than 0.2, most of GF deviations stay within 10%. When GF spread factor increases over 0.2, the GF deviation starts to increase up to 30%. Similar relationship is found between nf(NH+LH) and GF deviation, but the tendency is constrained within 10% and many outliers cannot be captured by increasing nf(NH+LH). This is because the relationship between nf(NH+LH) and GF spread factor is not linear. Certain aerosol populations, for example, external mixture of inorganics and sea-salt, that does not contain NH and LH mode, could exhibit a larger GF spread factor. It is also possible that aerosol with a small spread factor value can contain significant number of particles in NH and LH modes. Above all, we conclude that, although the scatter is larger, aerosol with a larger GF spread factor tend to be associated with high GF deviation. Two examples of GF-PDFs with a GF spread factor larger than 0.2 are shown in Fig. S6. These examples are suggesting the existence of multi-modal distribution. Comparing their chemical composition during C and M events, it was found the presence of sea-salt and elevated BC containing particles, as shown in Fig. S7, suggesting that the externally mixed and anthropogenically impacted aerosol and/or sea-salt containing polluted aerosol are responsible for the discrepancy. Therefore, we suggest that great care must be exercised in estimating hygroscopicity with bulk PM1 chemical composition, when BC exceeds 0.1 μg m^{-3} and sea-salt is below 0.5 μg m^{-3}. It has to be noted that the frequency of occurrence of GF spread factor > 0.2 is as low as 1 % at Mace Head suggesting that, for most of the time, sea-salt containing bulk PM1 chemical composition can be used to achieve closure with aerosol hygroscopic properties.

4. Summary

In this study, data from an HTDMA and an AMS deployed at Mace Head atmospheric research station were used to characterize aerosol hygroscopicity and to elucidate the link with aerosol chemical composition taking the advantage of high temporal resolution of the two instruments. In winter, a period of low biological activity at Mace Head, all sampled aerosols

were mostly externally mixed, as revealed by the growth factor probability distribution functions. The continental and marine air masses were examined in detail in terms of the influence of chemical components on aerosol GFs and marine aerosol had significantly higher hygroscopicity than continental aerosol. A general agreement was achieved between estimated and measured growth factors for 165 nm aerosols. For continental events aerosols, a general agreement was achieved between estimated and measured hygroscopicity GF for D_0 165 nm aerosol, while for marine aerosols, the GF of particles larger than 75 nm could be estimated reasonably. A closure between hygroscopicity and chemical composition was achieved for the first time for marine aerosol with large sea-salt mass loading without significant systematic errors. The ZSR rule for hygroscopicity estimation of marine aerosol was validated for the first time with sea-salt measured by HR-ToF-AMS.

The analysis on statistical deviations from the perfect closure indicated that the highly external mixing state (GF spread factor > 0.2) can have the largest impact when comparing hygroscopicity derived from bulk chemical composition data and size-dependent hygroscopicity measurements. This study opens up new opportunities for predicting the physico-chemical properties of marine aerosols with HR-ToF-AMS. It should be noted that the good closure for marine aerosol has only been validated for winter time, and has yet to be explored for summer time when both primary and secondary biogenic organic matter concentrations are expected to be at their highest due to enhanced ocean biological productivity.

Author contributions

Colin O'Dowd and Darius Ceburnis conceived the study, Wei Xu analysed the data, Jurgita Ovadnevaite provided the AMS data, Wei Xu and Kirsten N. Fossum prepared the manuscript with the contribution from all co-authors.

Acknowledgements

Authors acknowleged Dr. Jakub Bialek for acquiring HTDMA data. Chinese Scholarship Council (No. 201706310154) is acknowledged for the fellowship of Mr. Wei Xu. The authors also like to acknowledge EPA-Ireland (AEROSOURCE, 2016-CCRP-MS-31), the COST Action CA16109 (COLOSSAL) and MaREI (Marine and Renewable Energy Ireland).

References

Asmi, E., Frey, A., Virkkula, A., Ehn, M., Manninen, H. E., Timonen, H., Tolonen-Kivimäki, O., Aurela, M., Hillamo, R. and Kulmala, M.: Hygroscopicity and chemical composition of Antarctic sub-micrometre aerosol particles and observations of new particle formation, Atmos. Chem. Phys., 10(9), 4253–4271, doi:10.5194/acp-10-4253-2010, 2010.

Berg, O. H., Swietlicki, E. and Krejci, R.: Hygroscopic growth of aerosol particles in the marine boundary layer over the Pacific and Southern Oceans during the First Aerosol Characterization Experiment (ACE 1), J. Geophys. Res. Atmos., 103(D13), 16535–16545, doi:10.1029/97JD02851, 1998.

Bialek, J., Dall'Osto, M., Monahan, C., Beddows, D. and O'Dowd, C. D.: On the contribution of organics to the North East Atlantic aerosol number concentration, Environ. Res. Lett., 7(4), 044013, doi:10.1088/1748-9326/7/4/044013, 2012.

Bialek, J., Dall'Osto, M., Vaattovaara, P., Decesari, S., Ovadnevaite, J., Laaksonen, A. and O'Dowd, C. D.: Hygroscopic and

430   chemical characterisation of Po Valley aerosol, Atmos. Chem. Phys., 14(3), 1557–1570, doi:10.5194/acp-14-1557-2014, 2014.

Chang, R. Y. W., Slowik, J. G., Shantz, N. C., Vlasenko, A., Liggio, J., Sjostedt, S. J., Leaitch, W. R. and Abbatt, J. P. D.: The hygroscopicity parameter (κ) of ambient organic aerosol at a field site subject to biogenic and anthropogenic influences: relationship to degree of aerosol oxidation, Atmos. Chem. Phys., 10(11), 5047–5064, doi:10.5194/acp-10-5047-2010, 2010.

Ching, J., Fast, J., West, M. and Riemer, N.: Metrics to quantify the importance of mixing state for CCN activity, Atmos.
435   Chem. Phys., 17(12), 7445-7458, doi:10.5194/acp-17-7445-2017, 2017.

DeCarlo, P. F., Kimmel, J. R., Trimborn, A., Northway, M. J., Jayne, J. T., Aiken, A. C., Gonin, M., Fuhrer, K., Horvath, T., Docherty, K. S., Worsnop, D. R. and Jimenez, J. L.: Field-Deployable, High-Resolution, Time-of-Flight Aerosol Mass Spectrometer, Anal. Chem., 78(24), 8281–8289, doi:10.1021/ac061249n, 2006.

DeCarlo, P. F., Slowik, J. G., Worsnop, D. R., Davidovits, P. and Jimenez, J. L.: Particle Morphology and Density
440   Characterization by Combined Mobility and Aerodynamic Diameter Measurements. Part 1: Theory, Aerosol Sci. Tech., 38(12), 1185–1205, doi:10.1080/027868290903907, 2004.

Duplissy, J., Gysel, M., Sjostedt, S. J., Meyer, N., Good, N., Kammermann, L., Michaud, V., Weigel, R., Martins dos Santos, S., Gruening, C., Villani, P., Laj, P., Sellegri, K., Metzger, A., McFiggans, G., Wehrle, G., Richter, R., Dommen, J., Ristovski, Z., Baltensperger, U. and Weingartner, E.: Intercomparison study of six HTDMAs: results and recommendations, Atmos.
445   Meas. Tech., 2(2), 363–378, doi:10.5194/amt-2-363-2009, 2009.

Fors, E. O., Swietlicki, E., Svenningsson, B., Kristensson, A., Frank, G. P. and Sporre, M.: Hygroscopic properties of the ambient aerosol in southern Sweden – a two year study, Atmos. Chem. Phys., 11(16), 8343–8361, doi:10.5194/acp-11-8343-2011, 2011.

Fossum, K. N., Ovadnevaite, J., Ceburnis, D., Dall'Osto, M., Marullo, S., Bellacicco, M., Simó, R., Liu, D., Flynn, M., Zuend,
450   A. and O'Dowd, C. D.: Summertime Primary and Secondary Contributions to Southern Ocean Cloud Condensation Nuclei, Sci. Rep., 8(1), 1295, doi:10.1038/s41598-018-32047-4, 2018.

Gysel, M., Crosier, J., Topping, D. O., Whitehead, J. D., Bower, K. N., Cubison, M. J., Williams, P. I., Flynn, M. J., McFiggans, G. and Coe, H.: Closure study between chemical composition and hygroscopic growth of aerosol particles during TORCH2, Atmos. Chem. Phys., 7(24), 6131–6144, doi:10.5194/acp-7-6131-2007, 2007.

455   Gysel, M., McFiggans, G. and Coe, H.: Inversion of tandem differential mobility analyser (TDMA) measurements, J. Aerosol Sci., 40(2), 134–151, doi:10.1016/j.jaerosci.2008.07.013, 2009.

Gysel, M., Weingartner, E. and Baltensperger, U.: Hygroscopicity of Aerosol Particles at Low Temperatures. 2. Theoretical and Experimental Hygroscopic Properties of Laboratory Generated Aerosols, Environ. Sci. Technol., 36(1), 63–68, doi:10.1021/es010055g, 2001.

460   Hong, J., Xu, H., Tan, H., Yin, C., Hao, L., Li, F., Cai, M., Deng, X., Wang, N., Su, H., Cheng, Y., Wang, L., Petaja, T. and Kerminen, V. M.: Mixing state and particle hygroscopicity of organic-dominated aerosols over the Pearl River Delta region in China, Atmos. Chem. Phys., 18(19), 14079–14094, doi:10.5194/acp-18-14079-2018, 2018.

Jimenez, J. L., Canagaratna, M. R., Donahue, N. M., Prevot, A. S. H., Zhang, Q., Kroll, J. H., DeCarlo, P. F., Allan, J. D., Coe, H., Ng, N. L., Aiken, A. C., Docherty, K. S., Ulbrich, I. M., Grieshop, A. P., Robinson, A. L., Duplissy, J., Smith, J. D., Wilson,
465   K. R., Lanz, V. A., Hueglin, C., Sun, Y., Tian, J., Laaksonen, A., Raatikainen, T., Rautiainen, J., Vaattovaara, P., Ehn, M., Kulmala, M., Tomlinson, J. M., Collins, D. R., Cubison, M. J., E, Dunlea, J., Huffman, J. A., Onasch, T. B., Alfarra, M. R., Williams, P. I., Bower, K., Kondo, Y., Schneider, J., Drewnick, F., Borrmann, S., Weimer, S., Demerjian, K., Salcedo, D.,

Cottrell, L., Griffin, R., Takami, A., Miyoshi, T., Hatakeyama, S., Shimono, A., Sun, J. Y., Zhang, Y. M., Dzepina, K., Kimmel, J. R., Sueper, D., Jayne, J. T., Herndon, S. C., Trimborn, A. M., Williams, L. R., Wood, E. C., Middlebrook, A. M., Kolb, C.
470 E., Baltensperger, U. and Worsnop, D. R.: Evolution of organic aerosols in the atmosphere, Science, 326(5959), 1525–1529, doi:10.1126/science.1180353, 2009.

Juranyi, Z., Tritscher, T., Gysel, M., Laborde, M., Gomes, L., Roberts, G., Baltensperger, U. and Weingartner, E.: Hygroscopic mixing state of urban aerosol derived from size-resolved cloud condensation nuclei measurements during the MEGAPOLI campaign in Paris, Atmos. Chem. Phys., 13(13), 6431–6446, doi:10.5194/acp-13-6431-2013, 2013.

475 Kaku, K. C., Hegg, D. A., Covert, D. S., Santarpia, J. L., Jonsson, H., Buzorius, G. and Collins, D. R.: Organics in the Northeastern Pacific and their impacts on aerosol hygroscopicity in the subsaturated and supersaturated regimes, Atmos. Chem. Phys., 6(12), 4101–4115, doi:10.5194/acp-6-4101-2006, 2006.

Kamilli1, K. A., Poulain, L., Held, A., Nowak, A., Birmili, W. and Wiedensohler, A.: Hygroscopic properties of the Paris urban aerosol in relation to its chemical composition, Atmos. Chem. Phys., 14(2), 737–749, doi:10.5194/acp-14-737-2014,
480 2014.

Kreidenweis, S. M. and Asa-Awuku, A.: Aerosol hygroscopicity: Particle water content and its role in atmospheric processes, in Treatise on Geochemistry, pp. 331–361. 2014.

Lambe, A. T., Onasch, T. B., Massoli, P., Croasdale, D. R., Wright, J. P., Ahern, A. T., Williams, L. R., Worsnop, D. R., Brune, W. H. and Davidovits, P.: Laboratory studies of the chemical composition and cloud condensation nuclei (CCN) activity
485 of secondary organic aerosol (SOA) and oxidized primary organic aerosol (OPOA), Atmos. Chem. Phys., 11(17), 8913–8928, doi:10.5194/acp-11-8913-2011, 2011.

Liu, B. Y. H., Pui, D. Y. H., Whitby, K. T., Kittelson, D. B., Kousaka, Y. and McKenzie, R. L.: the aerosol mobility chromatograph: a new detectoer for sulfuric acid aerosols, Atmos. Environ., 12(1-3), 99–104, doi:10.1016/0004-6981(78)90192-0, 1978.

490 Mahish, M. and Collins, D. R.: Analysis of a multi-year record of size-resolved hygroscopicity measurements from a rural site in the U.S, Aerosol Air Qual. Res., 17(6), 1489–1500, doi:10.4209/aaqr.2016.10.0443, 2017.

Massoli, P., Lambe, A. T., Ahern, A. T., Williams, L. R., Ehn, M., Mikkila, J., Canagaratna, M. R., Brune, W. H., Onasch, T. B., Jayne, J. T., Petaja, T., Kulmala, M., Laaksonen, A., Kolb, C. E., Davidovits, P. and Worsnop, D. R.: Relationship between aerosol oxidation level and hygroscopic properties of laboratory generated secondary organic aerosol (SOA) particles,
495 Geophys. Res. Lett., 37, L24801, doi:10.1029/2010GL045258, 2010.

Middlebrook, A. N., Bahreini, R., Jimenez, J. L. and Cangaratna M. R.: Evaluation of composition-dependent collection efficiencies for the Aerodyne Aerosol Mass Spectrometer using field data, Aerosol Sci. Tech., 46(3), 258-271, doi: DOI: 10.1080/02786826.2011.620041, 2012.

Nakao, S.: Why would apparent κ linearly change with O/C? Assessing the role of volatility, solubility, and surface activity of
500 organic aerosols, Aerosol Sci. Tech., 51(12), 1377–1388, doi:10.1080/02786826.2017.1352082, 2017.

O'Connor, T. C., Jennings, S. G. and O'Dowd, C. D.: Highlights of fifty years of atmospheric aerosol research at Mace Head, Atmos. Res., 90(2-4), 338–355, doi:10.1016/j.atmosres.2008.08.014, 2008.

O'Dowd, C. D. and de Leeuw, G.: Marine aerosol production: a review of the current knowledge, Philosophical Transactions of the Royal Society of London A: Mathematical, Physical and Engineering Sciences, 365(1856), 1753–1774,
505 doi:10.1098/rsta.2007.2043, 2007.

O'Dowd, C. D., Facchini, M. C., Cavalli, F., Ceburnis, D., Mircea, M., Decesari, S., Fuzzi, S., Yoon, Y. J. and Putaud, J.-P.: Biogenically driven organic contribution to marine aerosol, Nature, 431(7009), 676–680, doi:10.1038/nature02959, 2004.

O'Dowd, C. D., Ceburnis, D., Ovadnevaite. J., Vaishya, A., Rinaldi. M. and Facchini, M. C.: Do anthropogenic, continental or coastal aerosol sources impact on a marine aerosol signature at Mace Head?, Atmos. Chem. Phys., 14, 10687-10704, doi:10.5194/acp-14-10687-2014, 2014.

Ovadnevaite, J., Ceburnis, D., Canagaratna, M., Berresheim, H., Bialek, J., Martucci, G., Worsnop, D. R. and O'Dowd, C. D.: On the effect of wind speed on submicron sea salt mass concentrations and source fluxes, J. Geophys. Res. Atmos., 117, D16201, doi:10.1029/2011jd017379, 2012.

Ovadnevaite, J., Ceburnis, D., Leinert, S., Dall'Osto, M., Canagaratna, M., O'Doherty, S., Berresheim, H. and O'Dowd, C. D.: Submicron NE Atlantic marine aerosol chemical composition and abundance: Seasonal trends and air mass categorization, J. Geophys. Res. Atmos., 119(20), 11,850–11,863, doi:10.1002/2013JD021330, 2014.

Ovadenvaite, J., Manders, A., de Leeuw, G., Ceburnis, D., Monahan, C., Partanen, A.-I., Korhonen, K. and O'Dowd, C. D.: A sea spray aerosol flux parameterization encapsulating wave state. Atmos. Chem. Phys., 14, 1837-1852, doi:10.5194/acp-14-1837-2014, 2014.

Petters, M. D. and Kreidenweis, S. M.: A single parameter representation of hygroscopic growth and cloud condensation nucleus activity, Atmos. Chem. Phys., 7(8), 1961–1971, doi:10.5194/acp-7-1961-2007, 2007.

Petzold, A. and Schönlinner, M.: Multi-angle absorption photometry—a new method for the measurement of aerosol light absorption and atmospheric black carbon, J. Aerosol Sci., 35(4), 421–441, doi:10.1016/j.jaerosci.2003.09.005, 2004.

Quinn, P. K., Bates, T.S., Coffman, D.J., L. Upchurch, L., Johnson, J. E., Moore, R., Ziemba, L., Bell, T. G., Saltzman, E.S., Graff, J. and Behrenfeld, M. J.:Seasonal variations in western North Atlantic remote marine aerosol properties, J. Geophys. Res. Atmos., 124(24),14,240 – 14,261, doi:10.1029/2019JD031740, 2019.

Rader, D. J. and McMurry, P. H.: Application of the tandem differential mobility analyzer to studies of droplet growth or evaporation, J. Aerosol Sci., 17(5), 771–787, doi:10.1016/0021-8502(86)90031-5, 1986.

Rissler, J., Vestin[1], A., Swietlicki, E., G. Fisch, G., Zhou, J., Artaxo, P., and Andreae, M. O.:Size distribution and hygroscopic properties of aerosol particles from dry-season biomass burning in Amazonia, Atmos. Chem. Phys., 6(2), 471–491, doi: 1680-7324/acp/2006-6-471, 2006.

Rolph, G., Stein, A. and Stunder, B.: Real-time Environmental Applications and Display sYstem: READY, Environ. Modell. Softw., 95, 210–228, doi:10.1016/j.envsoft.2017.06.025, 2017.

Stokes, R. H. and Robinson, R. A.: Interactions in Aqueous Nonelectrolyte Solutions. I. Solute-Solvent Equilibria, J. Phys. Chem., 70(7), 2126–2131, doi:10.1021/j100879a010, 1966.

Stolzenburg, M. R. and McMurry, P. H.: TDMAFIT User's Manual, University of Minnesota, Department of Mechanical Engineering, Particle Technology Laboratory. 1988.

Su, H., Rose, D., Cheng, Y., Gunthe, S. S., Atmospheric, A. M., Stock, M., Wiedensohler, A., Andreae, M. O. and Poschl, U.: Hygroscopicity distribution concept for measurement data analysis and modeling of aerosol particle mixing state with regard to hygroscopic growth and CCN activation, Atmos. Chem. Phys., 10(15), 7489–7503, doi:10.5194/acp-10-7489-2010, 2010.

Suda, S. R., Petters, M. D., Yeh, G. K., Strollo, C., Matsunaga, A., Faulhaber, A., Ziemann, P. J., Prenni, A. J., Carrico, C. M., Sullivan, R. C. and Kreidenweis, S. M.: Influence of functional groups on organic aerosol cloud condensation nucleus activity, Environ. Sci. Technol., 48(17), 10182–10190, doi:10.1021/es502147y, 2014.

545 Swietlicki, E., Hansson, H. C., Hämeri, K., Svenningsson, B., Atmospheric, A. M., McFiggans, G., McMurry, P. H., Petaja, T., Tunved, P., Gysel, M., Topping, D. O., Weingartner, E., Baltensperger, U., Rissler, J., Wiedensohler, A. and Kulmala, M.: Hygroscopic properties of submicrometer atmospheric aerosol particles measured with H-TDMA instruments in various environments—a review, Tellus B Chem. Phys. Meteorol., 60(3), 432–469, doi:10.1111/j.1600-0889.2008.00350.x, 2008.

Swietlicki, E., Zhou, J., Berg, O. H., Martinsson, B. G., Frank, G., Cederfelt, S.-I., Dusek, U., Berner, A., Birmili, W., Wiedensohler, A., Yuskiewicz, B. and Bower, K. N.: A closure study of sub-micrometer aerosol particle hygroscopic 550 behaviour, Atmos. Res., 50(3-4), 205–240, doi:10.1016/s0169-8095(98)00105-7, 1999.

Swietlicki, E., Zhou, J., Covert, D. S., Hameri, K., Busch, B., Vakeva, M., Dusek, U., Berg, O. H., Wiedensohler, A., Aalto, P. P., Makela, J., Martinsson, B. G., Papaspiropoulos, G., Mentes, B., Frank, G. and Stratmann, F.: Hygroscopic properties of aerosol particles in the north- eastern Atlantic during ACE-2, Tellus B Chem. Phys. Meteorol., 52(2), 201–227, doi:10.1034/j.1600-0889.2000.00036.x, 2000.

555 Tang, M. J., Chan, C. K., Li, Y. J., Su, H., Ma, Q. X., Wu, Z. J., Zhang, G. H., Wang, Z., Ge, M. F., Hu, M., He, H., and Wang, X. M.: A review of experimental techniques for aerosol hygroscopicity studies, Atmos. Chem. Phys., 19, 12631-12686, doi: 10.5194/acp-19-12631-2019, 2019.

Tang, M., Guo, L., Bai, Y., Huang, R.-J., Wu, Z., Wang, Z., Zhang, G., Ding, X., Hu, M., Wang, X.: Impacts of methanesulfonate on the cloud condensation nucleation activity of sea salt aerosol. Atmos. Environ., 201:13-17, doi: 560 10.1016/j.atmosenv.2018.12.034, 2018.

Twomey, S.: Pollution and the planetary albedo, Atmos. Environ., 8(12), 1251–1256, doi:10.1016/0004-6981(74)90004-3, 1974.

Twomey, S.: The influence of pollution on the shortwave abedo of clouds, Journal of the Atmospheric Sciences, 34(7), 1149–1152, doi:10.1175/1520-0469(1977)034<1149:tiopot>2.0.co;2, 1977.

565 Wang, Y., Li, Z., Zhang, Y., Du, W., Zhang, F., Tan, H., Xu, H., Jin, X., Fan, X., Dong, Z., Wang, Q. and Sun, Y.: Characterization of aerosol hygroscopicity, mixing state, and CCN activity at a suburban site in the central North China Plain, Atmos. Chem. Phys. Discuss., 1–34, doi:10.5194/acp-2017-1100, 2018.

Wong, J. P. S., Lee, A. K. Y., Slowik, J. G., Cziczo, D. J., Leaitch, W. R., Macdonald, A. and Abbatt, J. P. D.: Oxidation of ambient biogenic secondary organic aerosol by hydroxyl radicals: Effects on cloud condensation nuclei activity, Geophys. Res. 570 Lett., 38(22), L22805, doi:10.1029/2011GL049351, 2011.

Wu, Z. J., Zheng, J., Shang, D. J., Du, Z. F., Wu, Y. S., Zeng, L.-W., Wiedensohler, A. and Hu, M.: Particle hygroscopicity and its link to chemical composition in the urban atmosphere of Beijing, China, during summertime, Atmos. Chem. Phys., 16(2), 1123–1138, doi:10.5194/acp-16-1123-2016, 2016.

Yeung, M. C., Lee, B. P., Li, Y. J. and Chan, C. K.: Simultaneous HTDMA and HR-ToF-AMS measurements at the HKUST 575 Supersite in Hong Kong in 2011, J. Geophys. Res. Atmos., 119, 9864–9883, doi:10.1002/2013JD021146, 2014.

Zhou, J., Swietlicki, E., Berg, O. H., Aalto, P. P., Hameri, K., Nilsson, E. D. and Leck, C.: Hygroscopic properties of aerosol particles over the central Arctic Ocean during summer, J. Geophys. Res. Atmos., 106(D23), 32111–32123, doi:10.1029/2000JD900426, 2001.

Zieger, P., Väisänen, O., Corbin, J. C. and Partridge, D. G.: Revising the hygroscopicity of inorganic sea salt particles, Nat.
580 Comm., doi:10.1038/ncomms15883, 2017.

Zuend, A., Marcolli, C., Booth, A. M., Lienhard, D. M., Soonsin, V., Krieger, U. K., Topping, D. O., McFiggans, G., Peter, T. and Seinfeld, J. H.: New and extended parameterization of the thermodynamic model AIOMFAC: calculation of activity coefficients for organic-inorganic mixtures containing carboxyl, hydroxyl, carbonyl, ether, ester, alkenyl, alkyl, and aromatic functional groups, Atmos. Chem. Phys., 11(17), 9155–9206, doi:10.5194/acp-11-9155-2011, 2011.

585

Table 1. Density and GF (at 90% RH) of chemical species used in the closure study.

	Density kg m^{-3}	GF
$(NH_4)_2SO_4$	1769	1.71
NH_4HSO_4	1780	1.7
H_2SO_4	1830	2.05
NH_4NO_3	1720	1.81
Sea-salt	2165	2.22
MSA	1481	1.71#
Organics	1400	1.18*
BC	1650	1

#adapted from Fossum et al. 2018 and Tang et al., 2018.
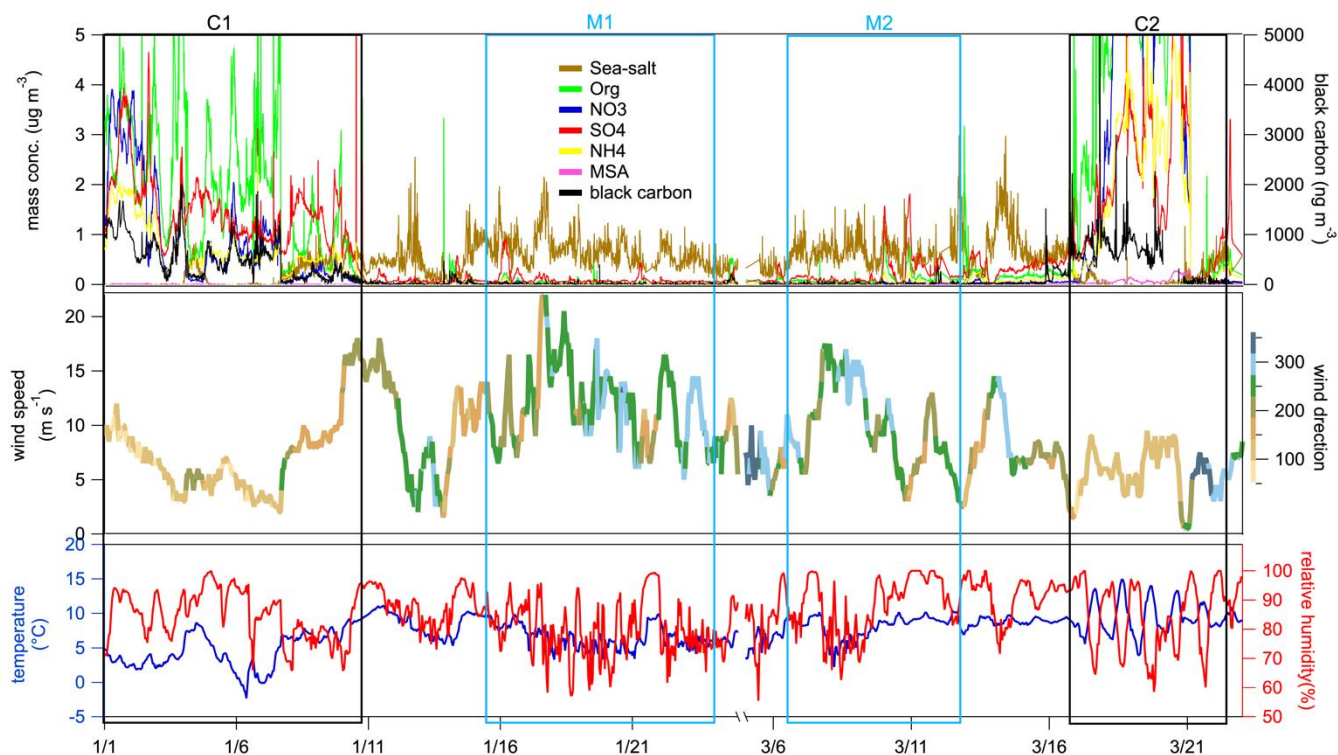
590 **Figure 1. Temporal variation of mass concentration of chemical species measured by the HR-ToF-AMS and MAAP (top panel); wind speed (m s^{-1}) with wind direction represented as a color-scale (middle panel); temperature (ºC, blue line, bottom panel) and RH (hPa, red line, bottom panel). Boxed areas correspond to continental events C1, C2 (in black) and marine events M1, M2 (in blue).**
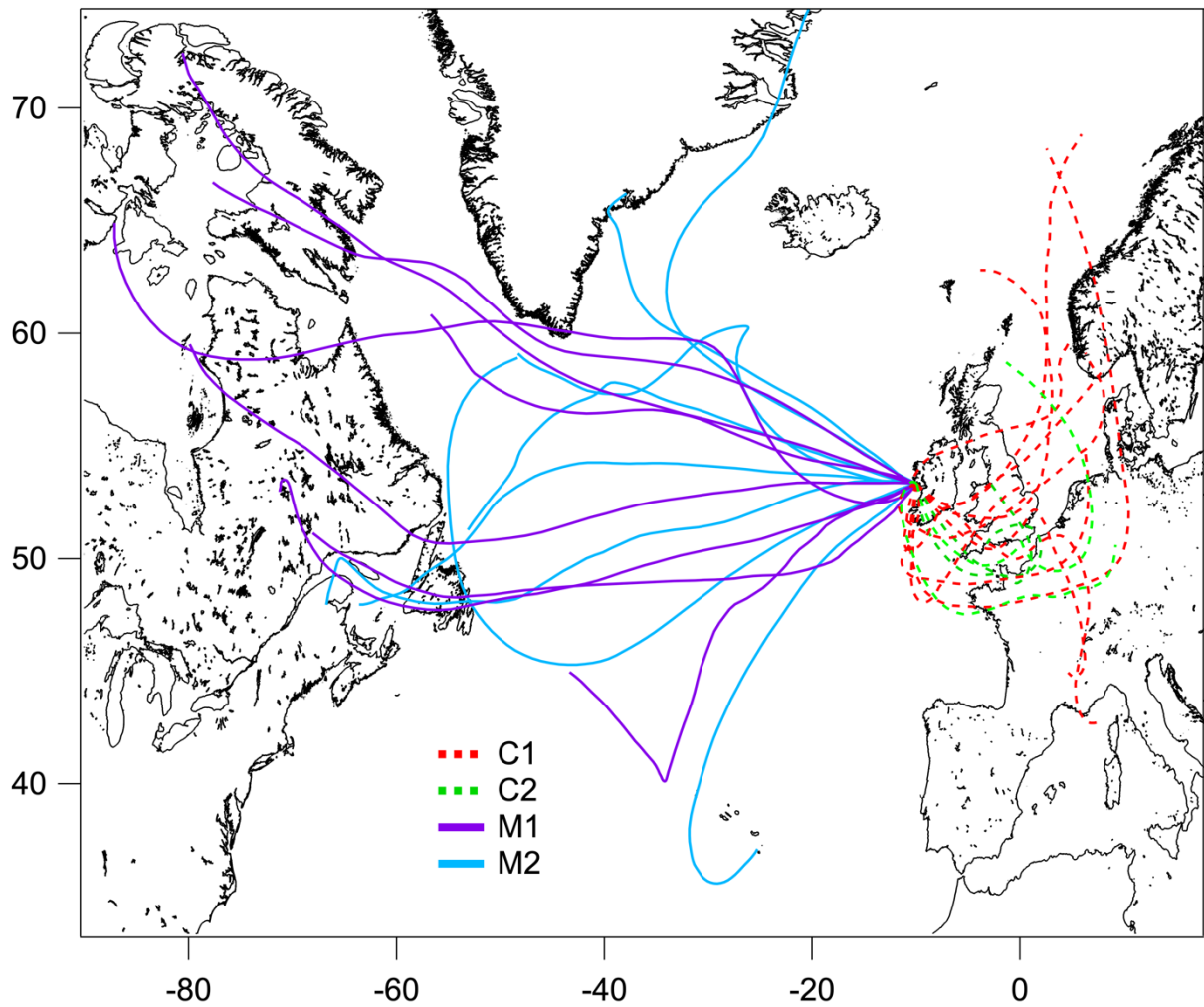
595

Figure 2. 72 h backward trajectories arriving at 500 m above mean sea level at Mace Head retrieved with Global Data Assimilation System for continental events (C1: red dash line, C2: green dash line) and marine events (M1: purple solid line, M2: purple solid line). The trajectory was calculated every 24 hours over the event duration.
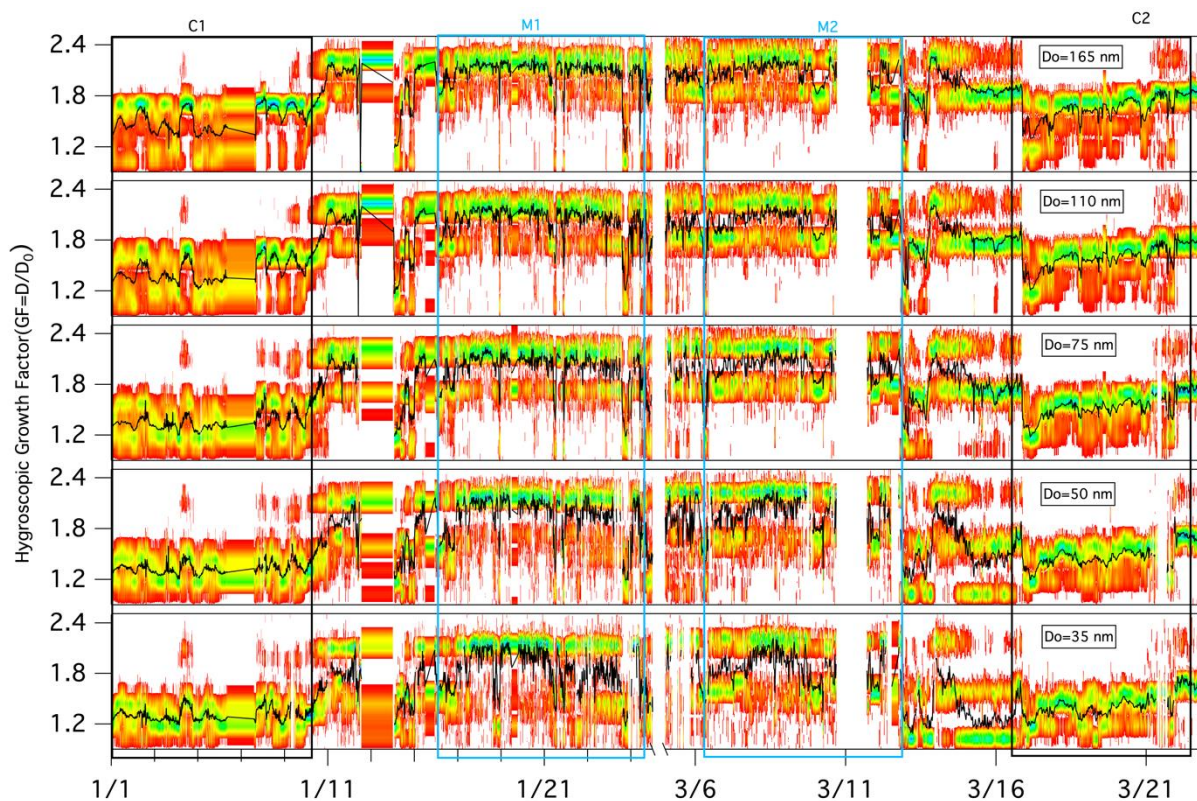
Figure 3. Growth factor probability distribution function (GF-PDF) for different particle dry sizes as measured by the HTDMA. The colour bar indicates the probability density and the black line represents the averaged GF.
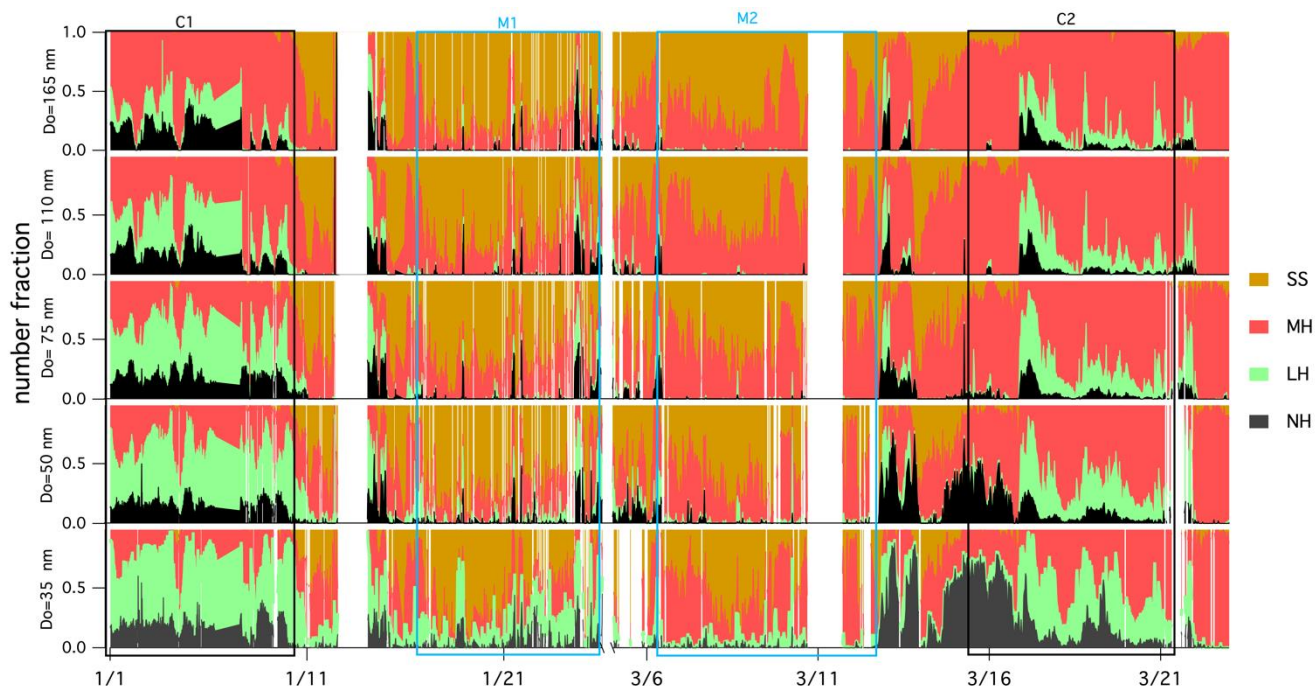
Figure 4. Time series of the number fraction of NH mode in black (GF<1.11), LH mode in green, (1.11<GF<1.33), MH mode in red(1.33<GF<1.85) and SS mode in brown (GF>1.85) of aerosols with pre-selected dry diameter.

605
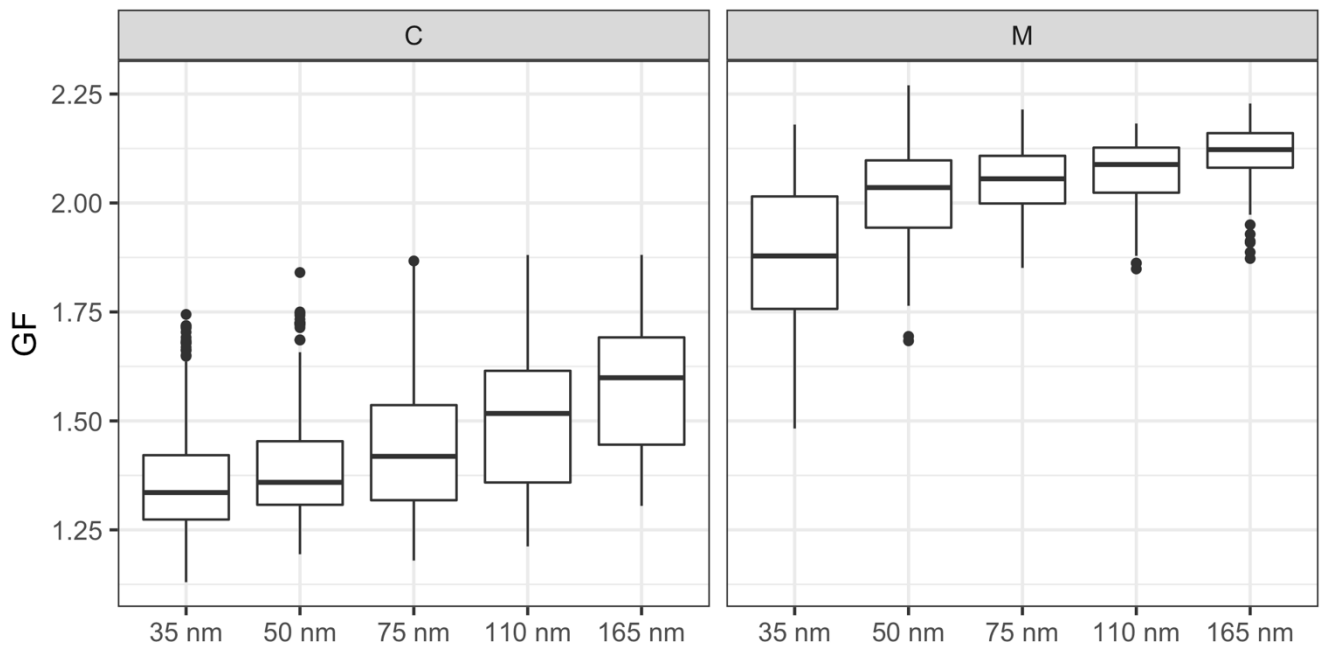
Figure 5. Size resolved GFs for (a) Continental (C) and (b) Marine (M). The horizontal lines represent median GF, the boxes represent 25-75 % percentile and whiskers represent 1.5*IQR from the boxes (where the IQR is the interquartile range). Data beyond the end of whisker are plotted individually as outliers.

610
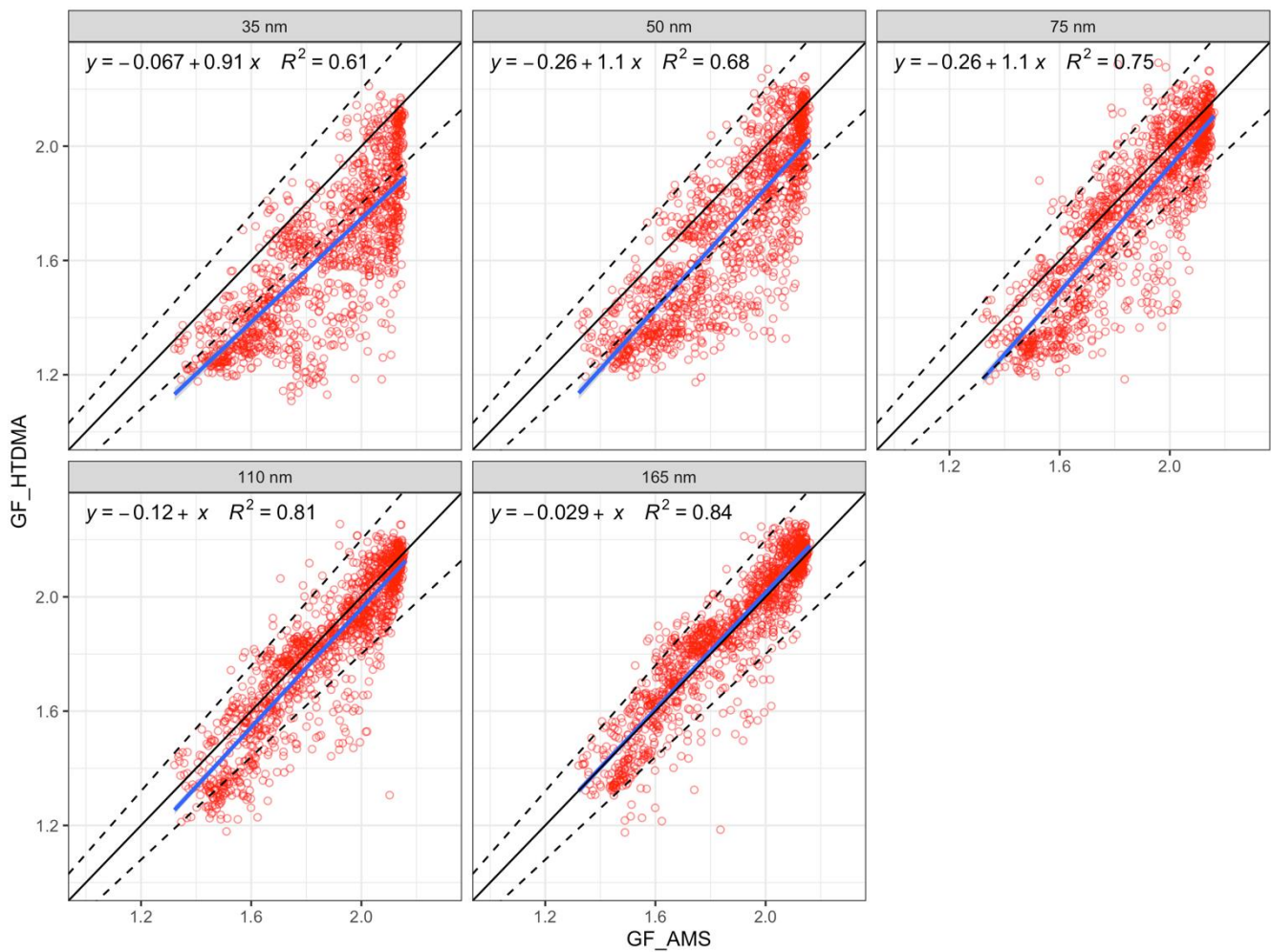
Figure 6. The comparison of bulk GF_AMS with size dependent GF_HTDMA. The 1:1 line is in black with a 10% deviation indicated by the dashed lines, blue line is the regression line: y=b + a*x, R² is the regression coefficient (variance).

615
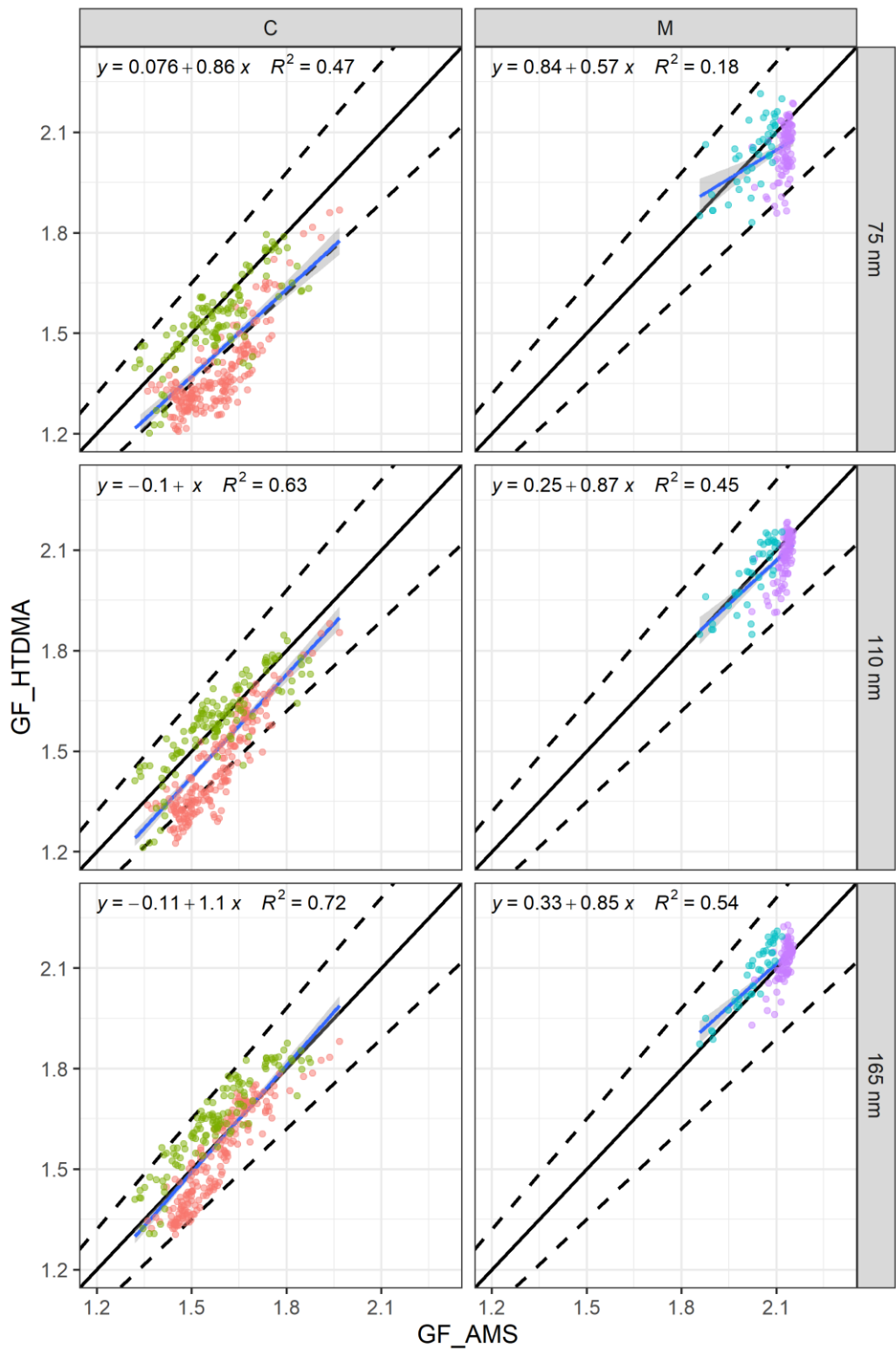
Figure 7. The relationship between GF-AMS and GF_HTDMA (D_0 = 75, 100 and 165 nm) of separated continental events (a, C1 in red, C2 in green) and marine events (b, M1 in blue, M2 in purple). Black line is 1:1 line for both Continental (C) or Marine (M) events, dash lines are 10% deviation and blue line is the regression equation.

620
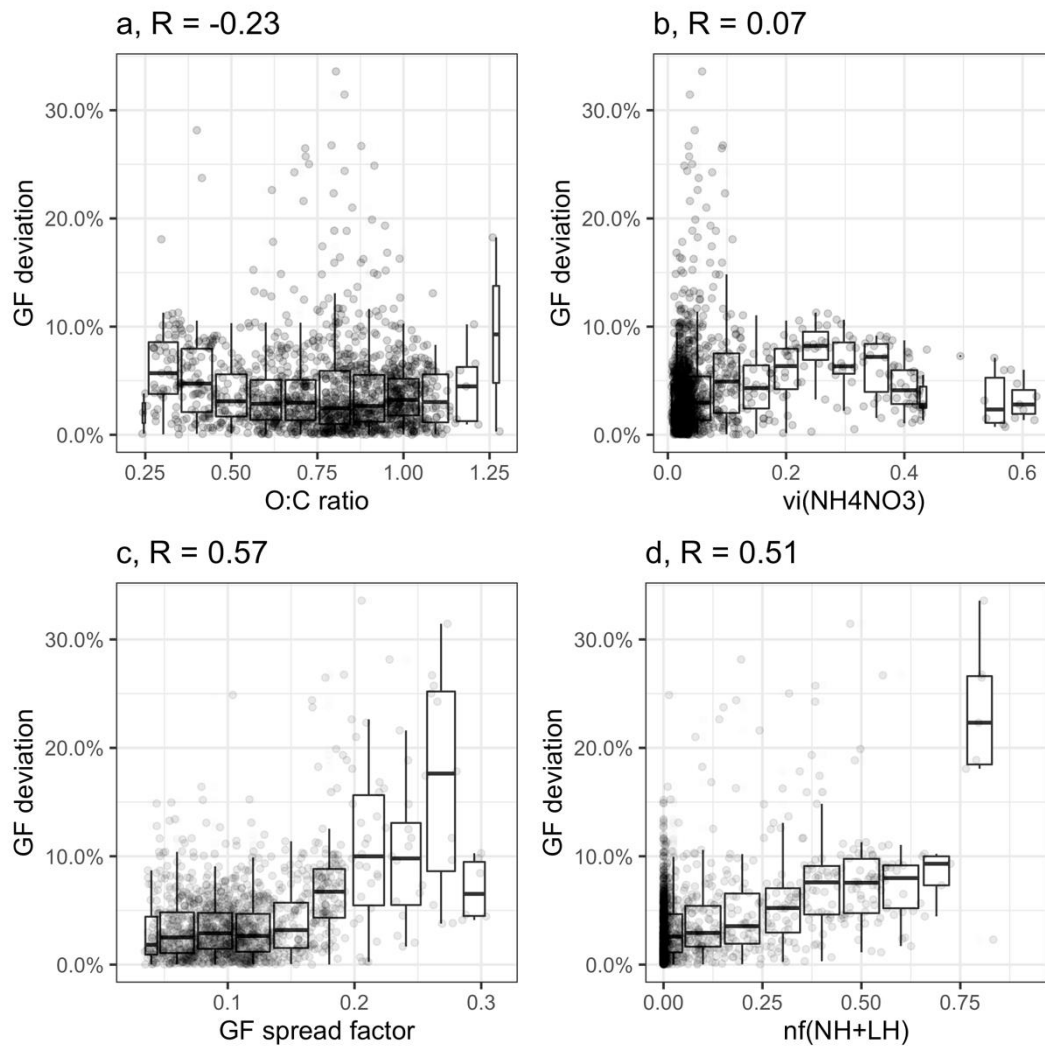
Figure 8. The relationship of GF deviation to (a) O:C ratio, (b) volume fraction of NH₄NO₃, c) GF spread factor and d) nf(NH+LH) over the whole period.